Early Optic Nerve Head Glial Proliferation and Jak-Stat Pathway Activation in Chronic Experimental Glaucoma

Diana C. Lozano, Tiffany E. Choe, William O. Cepurna, John C. Morrison, and Elaine C. Johnson

Casey Eye Institute, Oregon Health & Science University, Portland, Oregon, United States

Correspondence: Diana C. Lozano, Casey Eye Institute, Oregon Health & Science University, 3375 SW Terwilliger Boulevard, Portland, OR 97239-4197, USA; lozano@ohsu.edu.

Submitted: September 11, 2018
Accepted: January 25, 2019

Citation: Lozano DC, Choe TE, Cepurna WO, Morrison JC, Johnson EC. Early optic nerve head glial proliferation and Jak-Stat pathway activation in chronic experimental glaucoma. *Invest Ophthalmol Vis Sci*. 2019;60:921–932. https://doi.org/10.1167/iovs.18-25700

Purpose. We previously reported increased expression of cell proliferation and Jak-Stat pathway–related genes in chronic experimental glaucoma model optic nerve heads (ONH) with early, mild injury. Here, we confirm these observations by localizing, identifying, and quantifying ONH cellular proliferation and Jak-Stat pathway activation in this model.

Methods. Chronic intraocular pressure (IOP) elevation was achieved via outflow pathway sclerosis. After 5 weeks, ONH longitudinal sections were immunolabeled with proliferation and cell-type markers to determine nuclear densities in the anterior (unmyelinated) and transition (partially myelinated) ONH. Nuclear pStat3 labeling was used to detect Jak-Stat pathway activation. Nuclear density differences between control ONH (uninjected) and ONH with either early or advanced injury (determined by optic nerve injury grading) were identified by ANOVA.

Results. Advanced injury ONH had twice the nuclear density ($P < 0.0001$) of controls and significantly greater astrocyte density in anterior ($P = 0.0001$) and transition ($P = 0.006$) ONH regions. An increased optic nerve injury grade positively correlated with increased microglia/macrophage density in anterior and transition ONH ($P < 0.0001$, both). Oligodendroglial density was unaffected. In glaucoma model ONH, 80% of anterior and 66% of transition region proliferating cells were astrocytes. Nuclear pStat3 labeling significantly increased in early injury anterior ONH, and 95% colocalized with astrocytes.

Conclusions. Astrocytes account for the majority of proliferating cells, contributing to a doubled nuclear density in advanced injury ONH. Jak-Stat pathway activation is apparent in the early injury glaucoma model ONH. These data confirm dramatic astrocyte cell proliferation and early Jak-Stat pathway activation in ONH injured by elevated IOP.

Keywords: glaucoma, animal models, optic nerve, cell proliferation

Elevated intraocular pressure (IOP) is a well-documented glaucoma risk factor.[1,2] Several lines of evidence point to the lamina cribrosa of the optic nerve head (ONH) as the initial site of axonal injury in this disease.[3–5] Clinically, glaucoma is characterized by optic disc cupping, neuroretinal rim thinning, and progressive visual field loss. Glaucomatous human eyes demonstrate optic nerve axon and retinal ganglion cell loss accompanied by ONH remodeling and glial scarring.[4] Many of these pathophysiological changes are replicated in animal models of glaucoma in which IOP is either experimentally or genetically elevated.[4,6–9] Within the normal ONH, astrocytes are arranged into columns. Their processes are oriented perpendicular to retinal ganglion cell axons, separating them into bundles. Astrocytes are the most abundant glial cell type in the ONH, along with microglia. In the posterior ONH, oligodendroglia are increasingly prevalent as axons become myelinated. Both in human glaucoma and in animal glaucoma models with elevated IOP, astrocytes lose their typical arrangement and, along with microglia, alter their morphology.[10–17]

In addition to these morphologic changes, our previous studies have shown an upregulation of many cell proliferation–associated genes in glaucoma model ONHs.[18,19] To more fully understand the details of this observation, we previously quantified glaucoma model ONH DNA content and found that this increased between 117% (early injury) and 184% (advanced injury) compared to controls.[18,19] Furthermore, we showed by three-dimensional reconstructions that the mean ONH volume increased by 40% in early injury glaucoma model nerves.[20] These studies provide support for increased cellularity within the glaucomatous ONH but have yet to document cell proliferation or determine which ONH cells are involved in this process.

In addition to these proliferation findings, we found that minimally injured ONHs showed an upregulation of several interleukin-6 type cytokines (*Il6, Lif, Clcfl*) and *Socs3*, the feedback inhibitor of Stat3 phosphorylation (pStat3), suggesting an early activation of the Janus kinase and signal transducer and activator of transcription (Jak-Stat) pathway.[18,19] Jak-Stat pathway activation has been shown to regulate glial cell proliferation, as well as astrocytic differentiation, and this pathway may play an important role in the glial responses we have observed in pressure-induced injury.[17,18,21–25]

The purpose of this study is to answer hypotheses generated by our previous microarray work and identify, in chronic glaucoma model ONHs with early and advanced injury, the presence of proliferating (mitotic) cells and Jak-Stat pathway activation and determine which cells are involved.

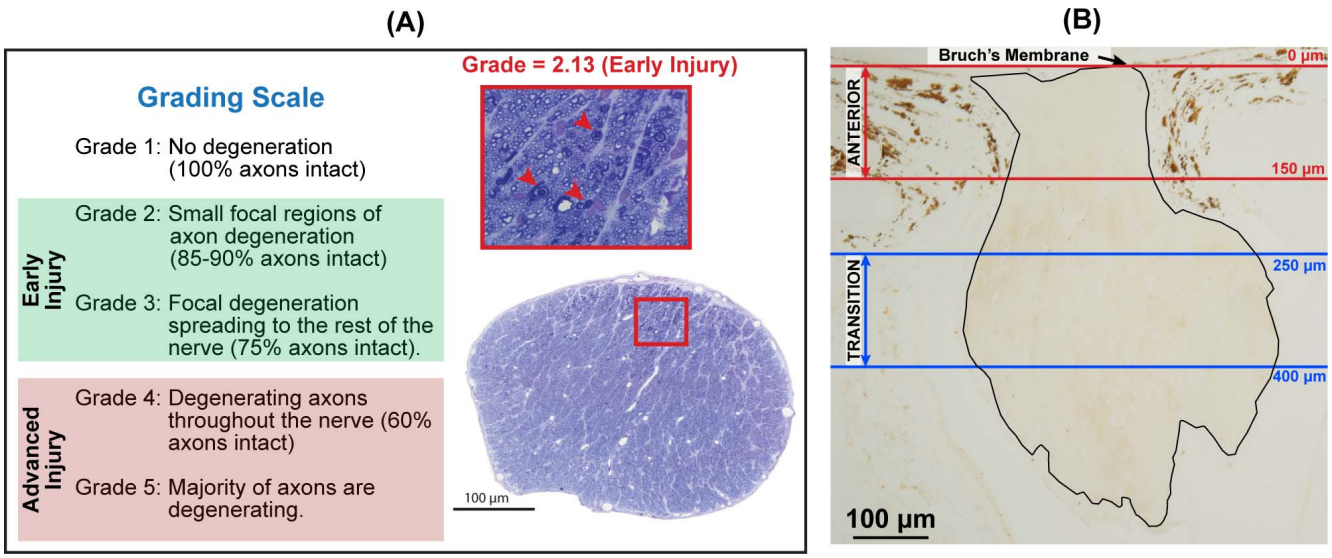

Figure 1. Optic nerve injury assessment and quantitative nuclear identification in the rat ONH. (**A**) Cross-sections of retrobulbar optic nerves (~1 mm behind the globe) were assessed for axonal injury in a scale from 1 (normal) to 5 (majority of axons in the process of degeneration). Images illustrate an optic nerve cross-section from a glaucoma model eye with early injury (grade = 2.13). The *red arrowheads* in the zoomed image (*red box*) indicate three degenerating axons. (**B**) Longitudinal ONH section. Nuclear densities were calculated in the anterior (between *red lines*; the first 150 µm posterior to BM) and transition ONH (between *blue lines*; from 250 to 400 µm posterior to BM). Note that the nerve bends out of the sectioning plane beyond the 400 µm line.

Methods

Chronic IOP Elevation and IOP Monitoring

All animal experiments were approved by the Oregon Health & Science University Institutional Animal Care and Use Committee and were performed in accordance with the Association for Research in Vision and Ophthalmology Statement for the Use of Animals in Ophthalmic and Vision Research. IOP was unilaterally elevated in 8-month-old, male retired breeder Brown Norway rats (N = 37) by a single episcleral vein injection of hypertonic saline.[26] IOP was measured with a rebound tonometer (TonoLab; Colonial Medical Supply, Franconia, NH, USA) in unanesthetized rats as previously described.[27] Animals were kept in constant dim light for the duration of the experiment, and IOP measurements were acquired prior to episcleral vein injection and at least three times a week for the duration of the experiment (5 weeks). IOP for each time point was calculated as the mean of 10 individual TonoLab readings. Mean IOP was then determined as the area under the curve of IOP (less the control fellow eye value) divided by the number of experimental days. Peak IOP was calculated as the maximum recorded measurement during the experimental period.

Optic Nerve Injury Grading

Animals were anesthetized and perfused transcardially with buffered 4% paraformaldehyde, as previously described.[26] Retrobulbar optic nerves (~1 mm behind the globe) were postfixed in buffered 5% glutaraldehyde and 1% osmium tetroxide, embedded in Spurr's resin, and cross-sectioned for light microscopic evaluation, as previously described.[19] Briefly, nerve cross-sections were stained with toluidine blue and graded for axonal injury on a scale from 1 (normal nerve) to 5 (majority of axons are in the process of degeneration; Fig. 1A). Each nerve was graded by three independent masked observers, and the mean of these grades defined the injury grade for that nerve. Nerves were then categorized into controls (uninjected eyes; grade = 1; N = 24) and two injected-eye groups based on the amount of axonal injury: early injury (grades < 3.5; N = 21) and advanced injury (grades ≥ 3.5; N = 16). Injury grades for individual nerves are presented in Supplementary Table S1.

It is important to note that axon degeneration was a very active and ongoing process in all nerves. In no nerve had degeneration progressed to the point that the remaining tissue was a glial scar.

ONH Immunohistochemistry

Globes, including the ONH, from the above animals were processed for ONH cell identification and quantitation. Globes were randomized into batches (each batch contained control and experimental globes), embedded in paraffin, and longitudinally sectioned vertically, with two sections per slide and 10 to 15 slides per globe. Slides were assigned into immunohistochemistry assay groups to include controls and globes with the full range of nerve injuries in each assay. Sections were immunolabeled with Ki67 or pStat3 and a cell type–specific antibody (Sox2, Iba1, etc.). All slides were labeled with DAPI (4′,6-diamidino-2-phenylindole). For the comparisons between anterior and transition regions, slides were selected that contained both, as illustrated in Figure 1. Not every eye was included in every analysis due to the limited number of sections per ONH and availability of appropriate sections for regional comparisons. The sample size for each analysis is provided in each table and figure.

Within each immunohistochemistry assay group, sections were deparaffinized, rehydrated in PBS, and blocked in either 5% goat (Vector Laboratories, Burlingame, CA, USA), horse (Vector Laboratories) or SEA BLOCK blocking buffer (ThermoFischer Scientific, Waltham, MA, USA) in PBS, and incubated overnight at 4°C with primary antibodies (Supplementary Table S2). For cell-type markers, primary antibodies used were goat anti-Sox2 (0.3 µg/mL; Santa Cruz Biotechnology, Santa Cruz, CA, USA) for astrocyte nuclei; rabbit anti-Pax2 (0.3 µg/mL; Invitrogen, Carlsbad, CA, USA) for astrocyte nuclei; anti-rabbit glial fibrillary acidic protein (anti-GFAP) (0.5 µg/mL;

Investigative Ophthalmology & Visual Science

DAKO, Carpinteria, CA, USA) for astrocytes; rabbit anti-Iba1 (anti-Aif1, 0.1 μg/mL; Wako Pure Chemical Industries Ltd., Richmond, VA, USA) for microglia/macrophage cells; and rabbit anti-Olig2 (1 μg/mL; Novus Biologicals, Littleton, CO, USA) for oligodendroglia nuclei. Also, mouse anti-Ki67 (usually 0.1 μg/mL, 2 μg/mL for colabeling with Iba1 only; DAKO) was used to identify mitotic nuclei and mouse anti-pStat3 (Tyr705, 1:100; Cell Signaling, Danvers, MA, USA) was used to detect activation of the Jak-Stat pathway.

As has been published previously, these specific primary antibodies were used for antigen immunolocalization in eye or central nervous system tissues as noted in Supplementary Table S2. Additional labeling was performed using the avidin-biotin technique with 3,3′-diaminobenzidine (DAB) chromogen with each primary antibody at the same concentrations as noted in Supplementary Table S2. We provide supplementary images of the cornea (Supplementary Fig. S1) and retina (Supplementary Fig. S2), using DAB to illustrate the specific and expected labeling with these antibodies elsewhere in the eye.

After primary antibody incubation, sections were washed in PBS, incubated for 30 minutes at room temperature in the appropriate 0.2% 488 anti-mouse IgG (Alexa Fluor 488; Life Technologies, Grand Island, NY, USA) and 0.2% anti-rabbit or anti-goat IgG (Alexa Fluor 594; Life Technologies) in blocking solution, washed again, and each slide was then coverslipped after applying a drop of antifade mounting media (Prolong Gold; Life Technologies) containing DAPI (used to identify nuclei). A control and glaucoma model ONH slide with the substitution of isotype IgGs for the primary antibodies at equivalent protein dilution were processed along with each assay as checks for nonspecific labeling (Supplementary Figs. S1 and S2). Each processed slide contained two sections, and the ONH section with the best morphology was photographed (at 20× magnification) with a fluorescence microscope (Olympus America, Center Valley, PA, USA) equipped with a digital camera and associated software (DP71; Olympus America). During all steps of this project, care was taken to avoid batch effects and to control for background fluorescence. For example, for each immunostaining assay, sections from each experimental group and IgG controls were processed simultaneously. Prior to acquiring images, the IgG control slides were viewed to determine background fluorescence. Then, control and experimental slides were briefly viewed to determine a standard camera exposure setting for each primary antibody tested. Once a standard exposure setting was selected, all photography was done at the same time using identical magnification.

For triple labeling, DAPI and the primary antibody Ki67 were used in combination with either Sox2, Pax2, Iba1, or Olig2 to identify the proportion of proliferating cells that colabeled with each cell type within the ONH. DAPI and primary antibody pStat3 were used in combination with Sox2 or Iba1 to identify activation of the Jak-Stat pathway within either astrocytes or microglia/macrophages, respectively. Lastly, to determine the specificity of Sox2 as an ONH astrocyte nuclear label, we used Sox2 in combination with GFAP, Pax2, Iba1, or Olig2 (Supplementary Fig. S3). We found that of $Sox2^+$-labeled nuclei, 86% colabeled with $GFAP^+$ cells, 41% with $Pax2^+$ nuclei, 2% with $Iba1^+$ cells, and 22% with $Olig2^+$ nuclei.

ONH Nuclear Identification and Quantitation

A program (Matlab R2015a and Image Processing Toolbox; The Mathworks, Inc., Natick, Massachusetts, USA) was developed to semiautomatically identify and quantitate ONH nuclei. We specifically compared and contrasted nuclear densities in the unmyelinated anterior ONH (from Bruch's membrane [BM] to 150 μm posterior to BM) and the partially myelinated transition ONH (from 250 to 400 μm posterior to BM; Fig. 1B).

This program was developed to colocalize $DAPI^+$ nuclear marker with labeling by each cell type antibody. This was accomplished by manually cropping the image to include only the desired ONH region. Image contrast for each color channel was independently and automatically adjusted by removing background noise, correcting for uneven background illumination, and improving image contrast. Each color channel was then thresholded at a standardized level. Given that the camera exposure settings during image acquisition were uniform, a standardized threshold level could be set for each tested primary antibody. In the event that the program yielded too many false positives (e.g., identification of nonnuclear structures), the user could manually adjust the threshold level until all appropriate nuclei were identified.

Nuclei centers were then identified using Matlab built-in functions, and the x- and y-coordinates for each identified nucleus were plotted back onto the ONH images to visually confirm that all appropriate nuclei were identified, allowing the user to add any nuclei missed by the program. These steps were repeated for all color channels independently, and colocalization was determined by multiplying the thresholded images together, such that a pixel value of one was plotted in the location of colabeled nuclei and zeros everywhere else. For example, nuclei that were $Sox2^+$ and $pStat3^+$ were identified by multiplying the thresholded DAPI, Sox2, and pStat3 images together as shown in Supplementary Figure S4. Finally, the x- and y-coordinates of cells that were manually added had to be within five pixels of a $DAPI^+$ location to count toward the final tally of nuclei.

For nonnuclear antibodies (Iba1 and GFAP), cells were counted when DAPI nuclei were completely surrounded by the label. $GFAP^+$ cells were manually counted because of the complex network of astrocyte labeling within the ONH.

For a subset of ONHs, nuclear densities calculated by the Matlab program were validated by comparing these semi-automated nuclear counts with manual counts performed by a second, independent observer (using Adobe Photoshop CS6 tools; Adobe Systems, San Jose, CA, USA). For this validation study, we focused on comparing anterior ONH nuclear densities done by both methods. An exception was made for Olig2, where nuclear densities in transition ONH were analyzed. There was excellent agreement ($P \geq 0.9$) between calculated nuclear densities provided by the two approaches for all primary antibodies (Supplementary Table S3).

Statistical Analysis

One-way ANOVA, followed by Dunnett's multiple comparison test, was used to identify differences in IOP or nerve injury grades between controls and early injury or advanced injury groups.

Nuclear counts were transformed to nuclear densities by dividing the total number of nuclei by the evaluated ONH area. When more than one section per eye was processed, nuclear densities from all sections for a given ONH and region were averaged. Due to the low number of Ki67-labeled nuclei in a given section, proliferating cell nuclear density was calculated by summing the total nuclei divided by the summed area. Where necessary, data were transformed to avoid violating the assumptions of ANOVA.[28–31] (However, the raw mean and standard error nuclear densities are reported in Table 2.) One-way ANOVA followed by Dunnett's multiple comparison test was used to identify differences between controls and either early injury or advanced injury groups. Nerves included in the ONH regional analysis (comparison between anterior and transition ONH) needed to be long enough to have a transition

Table 1. IOP History and Optic Nerve Grade by Injury Group

Groups	Mean ± SD	Peak IOP	ON Grade	*N*
Controls	22 ± 2	27 ± 3	1.0 ± 0.0	24
Early injury	23 ± 5	38 ± 10*	1.8 ± 0.9*	21
Advanced injury	30 ± 6*	55 ± 7*	4.8 ± 0.4*	16

Values are the mean ± standard deviation of the mean.
* Significantly different from respective controls ($P < 0.05$).

ONH region, and each nerve needed to have at least two sections processed and analyzed. Only a subset of samples met these criteria, and they are presented in Supplementary Table S4. Paired 2-way ANOVA, followed by Sidak's multiple comparisons test, was used to identify differences by ONH region among groups. All statistical analyses were performed using statistical software (GraphPad Prism, version 6.0; GraphPad Software, Inc., La Jolla, CA, USA).

Results

Elevated IOP and Optic Nerve Injury in Experimental Glaucoma Eyes

IOP parameters (mean IOP and peak IOP) and optic nerve injury grades for control, early injury, and advanced injury groups are summarized in Table 1 and Supplementary Figure S5. Mean IOP in advanced injury ($P = 0.0001$) and peak IOP in both early injury ($P < 0.0001$) and advanced injury ($P < 0.0001$) groups for the 5 weeks following hypertonic saline injection were significantly higher than controls, and duration of IOP elevation in the early injury group was less than in the advanced group. Similarly, nerve injury, as determined by optic nerve injury grade, was significantly greater than controls for both glaucoma model groups ($P < 0.0001$ for both). Additionally, more nerve injury was seen in advanced injury than in early injury ($P < 0.0001$).

In our previous microarray examination of ONH gene expression, we observed two dominant responses in ONH with early injury (less than 15% optic nerve degeneration), the upregulation of genes associated with cell proliferation and those associated with Jak-Stat signaling pathway.[18,19] We will first present evidence of cell proliferation in the glaucoma model ONH. Then we will use cell specific markers to quantitate changes in the glial composition of the rat ONH and determine the rate of glial cell proliferation. Finally, we will use colocalization of cell type–specific markers with pStat3 nuclear labeling as evidence of activation of the Jak-Stat pathway in these cells. All of these density data are provided in Table 2.

Increased ONH Cellularity With Advanced Glaucomatous Injury

The nuclear counterstain DAPI was used to identify and quantify total ONH nuclei. Glaucoma model ONHs with advanced injury had a twofold increase in nuclear densities in both the anterior ($P < 0.0001$) and transition ($P < 0.0001$) ONH relative to the control group (Fig. 2). Supplementary Figure S6 further illustrates increased cellularity in ONHs with advanced injury. There were no significant differences in $DAPI^+$ densities between anterior and transition regions within groups (Supplementary Table 4). Regional comparisons presented in this and the following Results paragraphs are based on analysis of data presented in Supplementary Table 4.

Table 2. ONH Nuclear Densities in Controls and in Glaucoma Model ONHs With Early Injury or Advanced Injury

ONH Location by Groups	Mean ± SEM, Nuclei/mm^2 (*N*)					
	DAPI	Ki67	Sox2	Pax2	Iba1	Olig2	pStat3
Anterior							
Controls	6,800 ± 339 (24)	8 ± 4 (14)	5,348 ± 231 (17)	4,349 ± 409 (10)	258 ± 20 (10)	16 ± 16 (6)	100 ± 49 (16)
Early injury	7,350 ± 443 (21)	216 ± 64 (14)*	5,103 ± 379 (19)	3,990 ± 255 (11)	485 ± 97 (11)*	63 ± 63 (11)	1,206 ± 352 (19)*
Advanced injury	15,417 ± 1,384 (16)*	136 ± 45 (9)*	9,823 ± 1,478 (11)*	4,992 ± 1,125 (7)	2,082 ± 329 (7)*	19 ± 19 (7)	1,037 ± 453 (9)*
Transition							
Controls	6,397 ± 377 (17)	20 ± 15 (10)	2,795 ± 274 (9)	1,735 ± 215 (4)	631 ± 129 (5)	2,387 ± 323 (7)	38 ± 24 (7)
Early injury	7,667 ± 268 (21)	154 ± 58 (16)	3,046 ± 174 (16)	1,773 ± 483 (11)	1,461 ± 278 (11)	1,691 ± 244 (13)	354 ± 169 (14)*
Advanced injury	14,124 ± 1,544 (15)*	52 ± 24 (10)	4,547 ± 581 (10)*	3,054 ± 707 (7)*	3,342 ± 476 (7)*	1,959 ± 363 (9)	541 ± 306 (9)*

* Indicates significant difference when compared to respective controls.

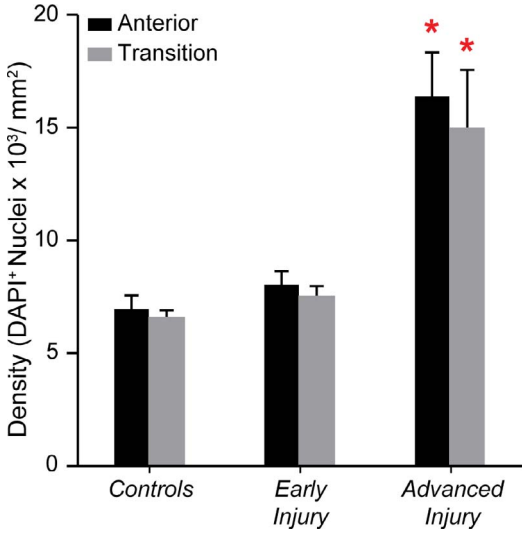

FIGURE 2. Increased cellularity in advanced injury glaucoma model ONH. Mean (±SEM) DAPI$^+$ nuclear densities in the anterior (*black bar*) and transition (*gray bar*) regions in controls ($N_{Anterior} = 24$; $N_{Transition} = 17$), early injury ($N_{Anterior} = 21$; $N_{Transition} = 21$), and advanced injury ($N_{Anterior} = 16$; $N_{Transition} = 15$) ONHs. The advanced injury group had significantly higher DAPI$^+$ densities in both the anterior ONH ($P < 0.0001$) and transition ONH ($P < 0.0001$) when compared to relative controls (*red asterisks*; Table 2). There was no significant difference between anterior and transition ONH densities within each group (Supplementary Table S4).

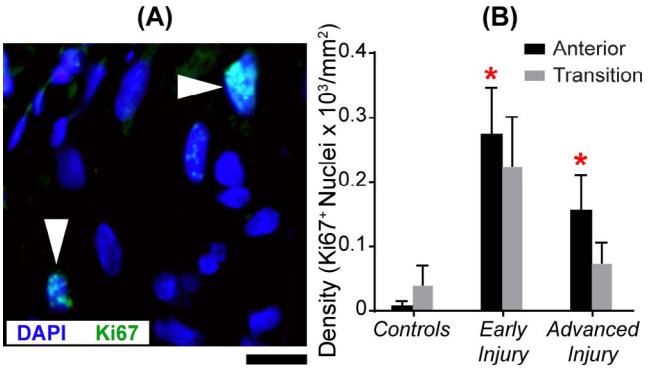

FIGURE 3. Significant increase in mitotic cell density in the anterior ONH of glaucoma model eyes. (**A**) Image of the anterior ONH with nuclear label DAPI (*blue*) and mitosis label Ki67 (*green*). *White arrowheads* point to two colabeled nuclei. *Scale bar*: 10 µm. (**B**) Mean (±SEM) Ki67$^+$ nuclear densities in the anterior (*black bar*) and transition (*gray bar*) region in controls ($N_{Anterior} = 14$; $N_{Transition} = 10$), early injury ($N_{Anterior} = 14$; $N_{Transition} = 16$), and advanced injury ($N_{Anterior} = 9$; $N_{Transition} = 10$) ONHs. There was a significant increase (*red asterisk*) in mitotic nuclei in the anterior ONH of the early injury ($P = 0.0006$) and advanced injury ($P = 0.001$) groups when compared to the controls (Table 2). There was no significant difference between anterior and transition ONH densities of mitotic cells within each group (Supplementary Table S4).

Cell Proliferation in Glaucoma Model ONH

To determine if the increased cellularity was, at least in part, due to cell proliferation, we immunostained ONH sections for the mitotic marker Ki67 (Fig. 3). Glaucoma ONHs with early injury ($P = 0.0006$) and advanced injury ($P = 0.001$) had significantly more proliferating nuclei than controls (Fig. 3; Table 2), with the highest values in ONHs with early injury. Note that the *y*-values shown in Figure 3 are a tenth of values plotted in other result figures, further indicating that a small proportion of nuclei are proliferating. Within groups, there were no significant differences between anterior and transition Ki67$^+$ nuclear densities (Supplementary Tables S4).

Astrocytic Proliferation in Glaucoma Model ONH

Next, we determined which ONH cells were proliferating in glaucomatous injury. Because astrocytes are the most common cells of the ONH, we first quantified astrocytes using three specific markers, GFAP, Sox2, and Pax2. GFAP is the most commonly used astrocyte marker. However, GFAP is less than satisfactory for quantitative studies in the ONH because it labels the cytoskeleton (rather than nuclei) and because of the complex intertwining of astrocyte processes in the ONH (see Supplementary Fig. S3).[15,32] Because of this, two additional nuclear markers, Sox2 and Pax2, which produced a more discrete nuclear label, were used. Sox2 is associated with the maintenance of neural stem cells in adult neurogenic areas,[33] which in the anterior ONH could only be astrocytes. Recently, Sox2 mRNA was identified as highly specific to astrocytes in the central nervous system.[34] Sox2 counts agreed best with our counts of GFAP-labeled cells in the anterior region of early injury ONH (4875 ± 376 and 4260 ± 469 cells/mm^2, respectively, $N > 8$). Furthermore, we found that that between 81% (anterior ONH) and 93% (transition ONH) of Sox2$^+$ nuclei were completely surrounded by GFAP-positive processes. Also, as observed in the mouse ONH,[35] we found Sox2 labeled about 15% more nuclei than Pax2 in the anterior ONH (see Supplementary Fig. S3). Therefore, we used Sox2 to quantify ONH astrocytes.

Advanced injury ONH had more Sox2$^+$ nuclei in the anterior ($P = 0.0001$) and transition ($P = 0.006$) regions than controls (Table 2). In regional comparisons within groups (Supplementary Table S4), there were approximately twice as many astrocytes (Sox2$^+$) in the anterior compared to the transition region of all groups (*P* values: controls = 0.03, early injury = 0.04, and advanced injury < 0.0001; Figs. 4A and 4B). Importantly, when colabeling of nuclei with Sox2 and Ki67 was examined in glaucoma model ONHs, we found that 80% (anterior) and 66% (transition) of mitotic cells labeled as astrocytes (Figs. 4C and 4D).

Microglia/Macrophage Density and Proliferation Rates in Glaucoma Model ONH

For ONH microglia, we used antibodies to Iba1, which also labels macrophages, such as tissue-resident macrophages.[36–39] To avoid changes in cellular morphology (in response to injury) leading to an overcount of Iba1$^+$ cells, we only counted DAPI$^+$ nuclei that were contiguous with the surrounding Iba1$^+$ label (Fig. 5). In general, we found that during active degeneration, the density of Iba1-labeled cells increased by more than fivefold in both ONH regions. Additionally, while Iba1-labeled cells were always most prevalent in the transition region, the proportion of mitotic Iba1 cells and the relative increase in Iba1 cell density was greatest in the anterior ONH.

More specifically, ONHs with advanced injury had more microglia/macrophages in the anterior ONH ($P = 0.01$) than controls. Additionally, the transition ONH with early injury ($P = 0.0001$) and advanced injury ($P = 0.0001$) had significantly more microglia/macrophages than their respective controls (Table 2). Also, when compared to ONHs with early injury, the advanced injury group had significantly more Iba1$^+$-

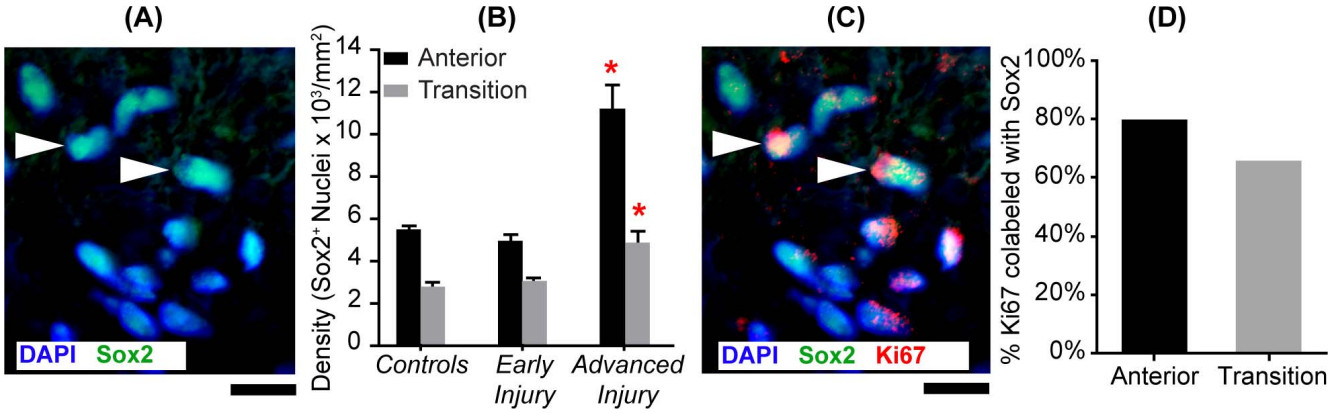

Figure 4. Astrocytes are the most abundant proliferating glia in glaucoma model ONH. (**A**) Image of the anterior ONH immunolabeled with astrocyte nuclear marker, Sox2. *White arrowheads* point to two of the astrocyte nuclei (identified by colocalization of Sox2 in *green* with DAPI in *blue*). *Scale bar*: 10 µm. (**B**) Mean (±SEM) $Sox2^+$ nuclear densities in the anterior (*black bars*) and transition (*gray bars*) regions in controls ($N_{Anterior} = 17$; $N_{Transition} = 9$), early injury ($N_{Anterior} = 19$; $N_{Transition} = 16$), and advanced injury ($N_{Anterior} = 11$; $N_{Transition} = 10$) ONHs. There were significantly more $Sox2^+$ nuclei in the anterior ($P = 0.0001$) and transition ($P = 0.006$) ONH of the advanced injury than controls (*red asterisk*; Table 2). There were also nearly twice as many astrocytes in the anterior compared to the transition ONH (*P* values: controls = 0.03, early injury = 0.04, and advanced injury <0.0001; Supplementary Table S4). (**C**) Image of the anterior ONH immunolabeled with Sox2 and Ki67 antibodies. *White arrowheads* point at two of the proliferating astrocytes as demonstrated by Sox2 (*green*) and Ki67 (*red*) nuclear colocalization. *Scale bar*: 10 µm. (**D**) In glaucoma model ONH, between 80% (anterior region) and 66% (transition region) of proliferating nuclei were astrocytes (colabeled with Sox2 and Ki67). There was negligible Ki67 labeling in control ONH.

labeled cells in both ONH locations ($P = 0.0006$ for anterior ONH and $P < 0.001$ for transition ONH). In both regions, we found $Iba1^+$ cell densities to be positively correlated with optic nerve injury grade (anterior: $r^2 = 0.65$, $P < 0.0001$, and transition: $r^2 = 0.68$, $P < 0.0001$). For regional comparisons within groups (Supplementary Table S4), the glaucoma model ONHs had more $Iba1^+$ cells in the transition region than the anterior ONH (*P* values: early injury = 0.03; advanced injury = 0.02).

When we examined colabeling of glaucoma model ONH with mitotic cell marker Ki67 and Iba1, we found approximately 14% (anterior) and 4% (transition) of $Ki67^+$ cells were colabeled as microglia/macrophage (Figs. 5C and 5D). Although there was a dramatic increase in $Iba1^+$ cells in the injured ONH, these cells were still the minority of proliferating cells in glaucoma model ONH.

Oligodendroglial Density in the Transition ONH and Lack of Proliferation in Glaucoma Model ONHs

The Olig2 antibody was used to identify oligodendroglial nuclei (Fig. 6). *Olig2* encodes a basic-helix-loop-helix protein that regulates the development of oligodendrocytes in vertebrates.[40–43] We found nearly all oligodendroglia in the transition ONH region, where densities did not differ significantly between controls and either experimental group (*P* values: early injury = 0.08 and advanced injury = 0.39). We found fewer than five $Olig2^+$ nuclei in the anterior ONH in three samples. These tended to be closer to the transition ONH, likely indicating that these eyes were sectioned at a slightly oblique angle. More importantly, we found no Olig2 and Ki67 colabeling, indicating that there was no detectable proliferation of oligodendroglia in the ONH.

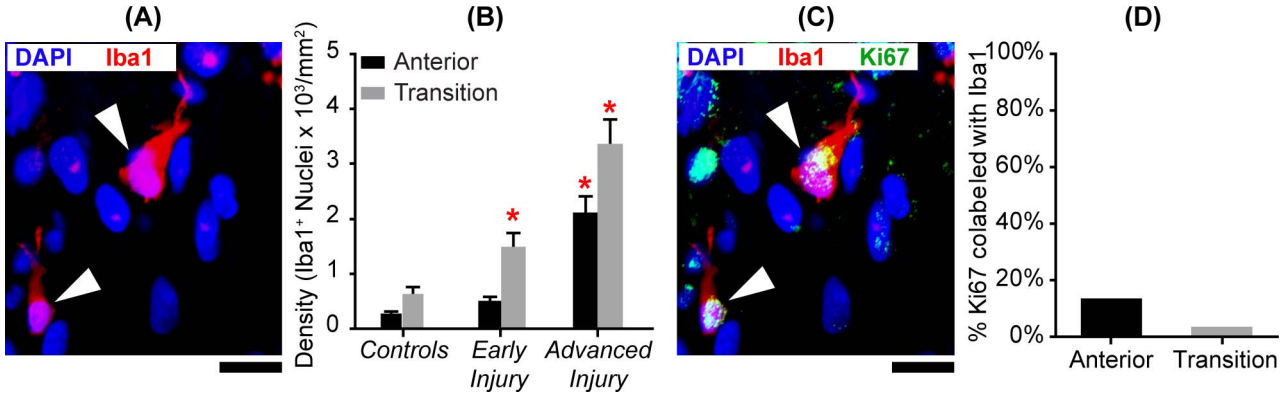

Figure 5. Microglia/macrophage density and proliferation in glaucoma model ONH. (**A**) Image of the anterior ONH immunolabeled for Iba1. *White arrowheads* point to two microglia/macrophages, identified by DAPI (*blue*) nucleus surrounded by Iba1 (*red*) labeling. *Scale bar*: = 10 µm. (**B**) Mean (±SEM) $Iba1^+$ cell densities in the anterior (*black bars*) and transition (*gray bars*) regions in controls ($N_{Anterior} = 10$; $N_{Transition} = 5$), early injury ($N_{Anterior} = 11$; $N_{Transition} = 11$), and advanced injury ($N_{Anterior} = 7$; $N_{Transition} = 7$) ONHs (see Table 2). Significantly more $Iba1^+$ cells were found in the transition ONH with early injury ($P = 0.0001$) and advanced injury ($P = 0.0001$), as well as in the anterior ONH with advanced injury ($P = 0.01$), compared to respective controls (*red asterisks*). Also, the transition ONH in both glaucoma model ONH groups had more $Iba1^+$ cells than the anterior ONH (*P* values: early injury = 0.03, advanced injury = 0.02; see Supplementary Table S4). (**C**) Image of the anterior ONH immunolabeled for Iba1 and Ki67. *White arrowheads* point to two proliferating microglia/macrophages (DAPI in *blue*, Iba1 in *red*, and Ki67 in *green*). *Scale bar*: 10 µm. (**D**) Density of $Ki67^+$ nuclei that labeled with $Iba1^+$ in the anterior and transition ONH. No more than 15% of $Ki67^+$ nuclei were $Iba1^+$.

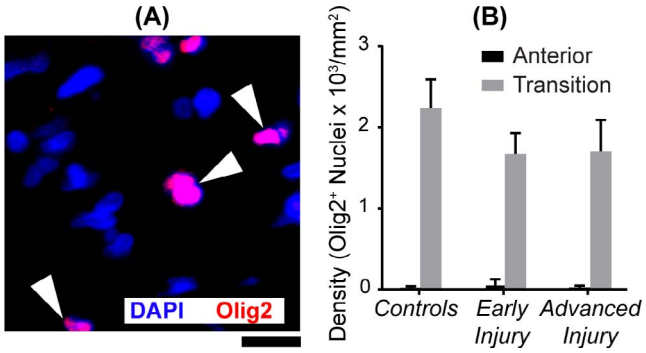

Figure 6. Oligodendroglial densities in transition region. (**A**) Image of the ONH transition region immunolabeled for Olig2. *White arrowheads* point to three oligodendroglial nuclei (e.g., colocalization of Olig2 in *red* and DAPI in *blue*). *Scale bar*: 10 µm. (**B**) Mean (±SEM) Olig2$^+$ nuclear densities in the transition ONH were not significantly altered by glaucomatous injury (Table 2). Sample size ranged between 6 and 11 in the anterior ONH and between 7 and 13 in the transition ONH. Negligible Olig2$^+$ nuclei were found in the anterior regions. We found no colabeling of mitotic marker Ki67$^+$ with Olig2$^+$.

Proportional Contribution of Astrocytes, Microglia/Macrophage, and Oligodendroglia to ONH Cellularity in Glaucoma Model ONHs

Figure 7 summarizes the proportional contribution of each cell type to the total number of ONH nuclei by injury group. In general, the proportion of astrocytes (Sox2$^+$ nuclei) decreased slightly in experimental glaucoma ONH, while the proportional contribution of microglia/macrophages (Iba1$^+$ nuclei) increased. In the transition region, the proportion of oligodendroglia progressively decreased with increasing injury. Additionally, an increasing proportion of nuclei did not label with glial-specific antibodies. These would include non-glial cells, such as fibroblasts, endothelial cells, and pericytes that contribute to the total population of ONH nuclei, as well as any glial cells that fail to express the selected markers.

Jak-Stat Pathway Activation, as Indicated by pSTAT3 Labeling, Primarily Colocalizes With Astrocyte Markers While Colabeling With Microglia/Macrophages is Negligible

In our previous microarray studies, axonal injury in early chronic glaucoma was associated with an upregulation of genes involved with the Jak-Stat pathway.[18] Activation of this pathway can occur when an Il6-type cytokine binds to transmembrane α and gp130 receptors, which then phosphorylates Jak2. Jak2 in turn phosphorylates Stat3 (pStat3). pStat3 homodimers translocate into the nucleus, activating transcription and regulating multiple downstream cell pathways, including proliferation.[44,45] Here we utilized the pStat3 antibody to localize activation of the Jak-Stat pathway (Fig. 8). Stat3 phosphorylation at this site is associated with canonical Stat3 signaling and astrocyte reactivity.[46]

Figure 8 shows that, when compared to their respective controls (Table 2), glaucoma model ONHs had significantly more pStat3$^+$ nuclei in both the anterior (*P* values: early injury = 0.009 and advanced injury = 0.03) and transition ONH (*P* values: early injury = 0.03 and advanced injury = 0.01). Also, in ONHs with early injury, there were nearly six times more pStat3$^+$ nuclei in the anterior compared to the transition region (*P* = 0.03).

Secondly, we determined if this activation colocalized with astrocytes (Sox2) and/or microglia/macrophages (Iba1). We found pStat3$^+$ nuclei almost exclusively colabeled with astrocytes. For example, in the anterior ONH with early injury, about 95% pStat3$^+$ nuclei colabeled with Sox2$^+$ and only 1% of pStat3$^+$ nuclei colabeled with Iba1$^+$ nuclei.

Discussion

This study confirms two hypotheses we proposed based on our previous analysis of gene expression changes in glaucoma model ONHs. These are that there is evidence of (1) cell proliferation and (2) Il6-type cytokine signaling via the Jak-Stat signaling pathway in ONHs with early injury.[18] Additionally, we demonstrate that, while both astrocytes and microglia/macro-

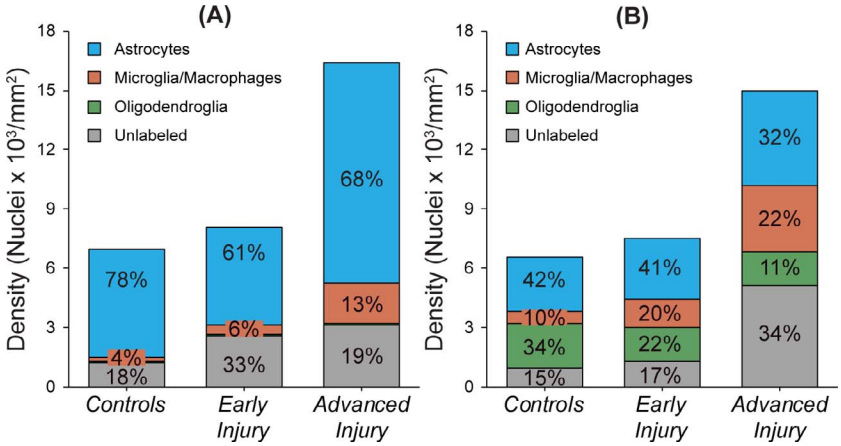

Figure 7. Cellular composition of control and glaucoma model ONH. Proportional contribution of astrocytes (Sox2$^+$, *blue*), microglia/macrophages (Iba1$^+$, *orange*), oligodendroglia (Olig2$^+$, *green*), and unlabeled (*gray*) nuclei in the (**A**) anterior and (**B**) transition ONH based on the average density of each cell type within each injury group. In the anterior, in both control and glaucoma model ONH, astrocytes are by far the predominant cell type. While the transition region includes oligodendroglia in addition to microglia/macrophage, the majority of nuclei in both control and glaucoma model ONH label as astrocytes as well. Unlabeled cells may include glial progenitor cells (such as NG2 cells), endothelial, and other non-glial cells.

Investigative Ophthalmology & Visual Science

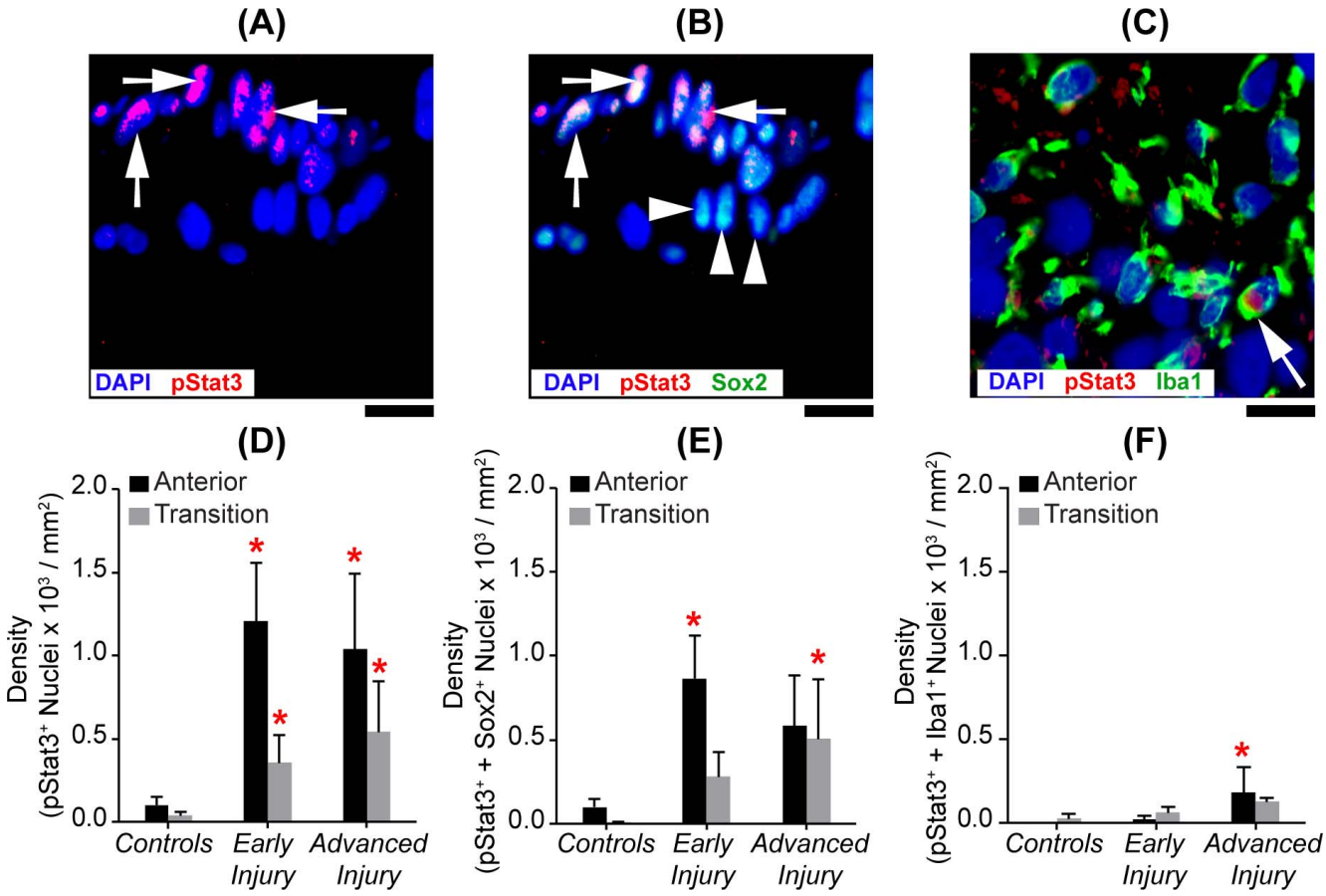

Figure 8. Predominant localization of Jak-Stat activation with astrocytes. Images of the anterior ONH region that were immunolabeled for (**A**) pStat3 alone (*red*), (**B**) pStat3 (*red*) and Sox2 (*green*), or (**C**) the transition ONH immunolabeled for pStat3 (*red*) and Iba1 (*green*). *Scale bar*: 10 μm. In (**B**), *white arrows* point out several $Sox2^+$ nuclei colabeled with $pStat3^+$, while other $Sox2^+$ nuclei (*white arrowheads*) lack pStat3 labeling. In (**C**), a different ONH section imaged in the transition region, and only one $Iba1^+$ cell (*white arrow*) colabeled with pStat3. Mean densities of ONH nuclei colabeling by group with (**D**) $pStat3^+$, (**E**) $pStat3^+$, and $Sox2^+$ and (**F**) $pStat3^+$ and $Iba1^+$ anterior (*black bars*) and transition (*gray bars*) ONH regions (mean ± SEM; sample size for controls: $N_{Anterior} = 16$ and $N_{Transition} = 7$; early injury: $N_{Anterior} = 19$ and $N_{Transition} = 14$; advanced injury $N_{Anterior} = 9$ and $N_{Transition} = 9$). *Red asterisks* indicate a significant difference ($P < 0.05$) from the respective controls.

phages proliferate in glaucoma model ONHs, the proliferation of astrocytes predominates.

Increases in cell density are not simply due to the loss of axons in these studies. In a previous study of axon counts versus injury grade in this model, we observed that only 15% of axons were injured in nerves with early injury.[47] Even in nerves with advanced injury, approximately 40% of axons were morphologically normal while axonal debris was in the initial stages of clearance. Importantly, three-dimensional reconstructions of early injury ONH from our model demonstrate that the volume of the ONH increases dramatically.[20] This increase is highly correlated with injury grade and results in an approximate doubling of the volume in ONHs with early injury (grade = 3) compared to controls. Note that the data presented in our current study are based on two-dimensional cell density measurements and, therefore, will actually underestimate the increased cellularity in the expanded volume of early glaucoma ONH.

Significant increases in the number of proliferating ONH cells, the majority of which were identified as astrocytes, were seen in the anterior region in both glaucoma model ONH injury groups. The nuclear Ki67 protein has been shown to be expressed for approximately 24 hours and during all phases of the cell division cycle, including in glial cells.[48–52] Ki67 protein is degraded in late mitosis and early G1 by the ubiquitin-proteasome system.[53] While the overall average percentage of cells that were proliferating at the time of tissue collection was only 2%, from the above it is reasonable to use this as an estimate of the daily rate of proliferation during the entire experimental period (35 days). This rate, applied to the density of $DAPI^+$ nuclei in control ONH (calculated mean advanced injury DAPI density = mean control DAPI density × 1.02^{35}) yields an approximate calculated final density of 13,000 to 14,000 nuclei/mm^2 and could account for much of the increase in cell density observed in ONHs with advanced injury (Table 2). These increases would also include proliferating microvascular cells, fibroblasts, or other cells that do not label with the cell-type markers that we utilized, as suggested by Figure 7. Another is the proliferation of NG2 (Cspg4+) glial cells, which are only present in the transition region of the rat[54] and have previously been reported to contribute to an increase in the number of oligodendrocytes in myelinated DBA/2J optic nerves with extensive axonal loss.[55]

While ischemia/reperfusion brain injury has been reported to induce astrocyte proliferation,[56,57] in our microarray study[18] quantifying ONH gene expression changes in nerves with pressures and injury similar to that of the current study, we found that expression of *Hif1* and *Epo* (two hypoxia-related markers) were not significantly different from controls in either early or advanced injury. This, along with optical coherence tomography angiography evidence that retinal and ONH blood flow are not compromised until IOP is well above

60 mm Hg,[58,59] suggests that the astrocyte proliferation observed here is unlikely to be simply a result of ischemia because peak IOPs do not exceed 60 mm Hg during the experimental time period (Supplementary Fig. S5).

As anticipated, we found that Iba1-labeled cells (microglia or macrophages) increased in density in injured ONH. Previously, we reported that these increases were correlated with mean IOP exposure,[39] so the proportional relationship to nerve injury reported here was not surprising. However, it is important to note that proliferating Iba1-labeled cells constituted a minority of the mitotic cells in both the anterior and transition ONH regions. In general, in the current study, the Iba1^{+} cell density did not significantly increase until axonal degeneration was advanced, indicating that microglia/macrophage densities are greatest when there is extensive axonal degeneration. Proliferation of these cells is a characteristic response to neural injury in the brain,[60,61] retina,[62–65] and optic nerve,[64,66,67] and microglial/macrophage proliferative responses have been studied in other glaucoma models in addition to ours. Using the laser photocoagulation model, Ebneter et al.[68] found activation of Iba1- and Ed1 (Cd68)-labeled cells in the retina, ONH, optic nerve, and optic tract, as evidenced by an increase in the labeled area that was correlated with the degree of axonal injury. Bosco et al.[12] demonstrated that early gliosis in DBA/2J mouse optic disks, as detected by confocal scanning laser ophthalmoscopy of CX3CR1+/GFP-labeled cells (microglia or macrophage), was correlated with the degree of optic nerve axonal degeneration. Lastly, it is important to point out that the increase in cell density reported here cannot be attributed primarily to monocytes, since cells labeled with the dual microglial/monocyte marker Iba1 remained a minor component of the ONH, particularly in the anterior region.

While alterations in astrocyte morphology have been documented in glaucoma model ONHs with early injury,[12,16] simultaneous increases in astrocyte density and proliferation in the ONH have not been carefully documented. We show here that astrocytes constitute the most abundant glial cell type in both the anterior and transition regions of the ONH. In our glaucoma model ONHs, during a time of active axon degeneration, astrocytes more than doubled in density in the anterior region. Additionally, astrocytes accounted for approximately 80% of mitotic glia in the anterior (unmyelinated) ONH and about 65% in the transition region.

When there is destruction of neural tissue, such as in spinal cord injuries[69] or cortical stab wounds,[70] up to 50% of affected astrocytes may divide within a few days and are thought to form a barrier between the lesion and surrounding tissue.[71] In some other types of neural injury, proliferation of microglia or oligodendroglia predominate whereas astrocyte proliferation is less,[60,72–76] including in the ONH following optic nerve transection.[66] The robust astrocytic proliferative response observed here by elevated IOP alone may be a unique aspect of early glaucomatous damage in the ONH. The predominance of these early responses in the anterior region, which is the site of the glial lamina and analogous to the primate lamina cribrosa, is consistent with the widely recognized observation that, in glaucoma, the lamina cribrosa is the primary site of injury.[3,77]

The overall impact of astrocyte proliferation on axon integrity in this glaucoma model is likely twofold. First, while undergoing cell division, astrocytes change in morphology and their specific gene and protein expressions are altered, all of which may compromise their ability to provide functional support to axons passing through the ONH.[13,16,18,78,79] In the ONH, as elsewhere in the nervous system, astrocytic functions include regulation of water and ion fluxes, support for action potential propagation, the provision of metabolic precursors via vascular interactions and glycogen storage, the supply of neurotrophic factors and antioxidants, the provision of communication and diffusion via gap junctions, the removal of cellular debris, and the generation of extracellular matrix.[54,80–87] Unmyelinated axons of the anterior ONH are particularly vulnerable to this decreased support due to their high metabolic demands.[88–91] Second, cell proliferation itself is an energy-consuming process that can double astrocyte glucose uptake.[92,93] Therefore, cell proliferation in the injured ONH is likely to place an additional metabolic stress on injured and remaining ONH axons.

In our microarray study, we identified upregulation of cell proliferation genes as well as genes associated with interleukin 6–type cytokines and the Jak-Stat signaling pathway.[18] Here we demonstrate that early in glaucomatous injury, the transcription factor, Stat3, is activated by phosphorylation in the ONH and that this occurs primarily in astrocytes. This labeling is most dramatic in conjunction with significant Ki67 labeling in these cells in the anterior region of the ONH, where the greatest increase in astrocyte density occurs. This suggests that Stat3 phosphorylation may signal astrocyte proliferation in response to elevated IOP injury. A key role for this pathway in astrocyte proliferation has been described in the spinal cord[94] and brain injury.[95]

Stat3 has been identified as necessary and sufficient for astrocyte differentiation and is a central regulator of astrocyte reactivity and proliferation.[46,94,96] Sun et al.[17] recently demonstrated pStat3 ONH labeling following various types of optic nerve injury in mice, including that following exposure to elevated IOP, similar to our report here. They also reported that the knockout of Stat3 in astrocytes attenuated astrocyte remodeling and decreased ganglion cell and axon survival as well as visual function following these injuries. In contrast, pharmacologic inhibition of ONH Stat3 following ischemic injury has been reported to increase axon survival in the optic nerve and retina, as well as ganglion cell survival.[97] In other neural tissues, Stat3 deletion or inhibition has been reported to reduce gliosis[98] and both reduce[99–102] and increase[103–105] neural injury. Therefore, while Stat3 phosphorylation may signal astrocytic proliferation in glaucoma model ONH, this has not been conclusively demonstrated, and the overall roles of Stat3 activation and the pathways that it may signal, including cell proliferation, in axonal degeneration warrant further clarification using other models of induced as well as experimental glaucoma.

One of the biggest challenges with any chronic experimental glaucoma model is that it is difficult to separate temporally early from late events. We, and others, have equated minimal focal injury with early injury and more widespread injury with advanced injury.[18,20,106–109] Still, the time course for these protein expression changes must be inferred, because IOP magnitude and duration cannot be precisely controlled. To address this problem, we recently developed a controlled elevation of IOP (CEI) model that produces many of the ONH message changes and axonal injury patterns seen previously in our chronic model.[110] The advantage of this approach is that pressure is elevated to a known level for a specific amount of time, and animals can be studied at any recovery time point following this exposure. In this new model, we showed that there is significant upregulation of various Il-6 type cytokines in the ONH during pressure elevation and that this precedes increases in cell proliferation–related genes (e.g., *Top2A* and *Prc1*), further supporting early involvement of the Jak-Stat pathway and consistent with the possibility that this drives cell proliferation. Further studies using this model are now underway to understand better the chronologic events leading to glial proliferation in the ONH and determine their relationship to axonal injury.

Acknowledgments

Supported by NIH/NEI Grants R01EY010145-17S1 (DCL), R01EY-010145 (JCM), R01EY-016866 (ECJ); and P30 EY010572 (OHSU), and by unrestricted departmental funding from Research to Prevent Blindness (New York, NY, USA).

Disclosure: **D.C. Lozano**, None; **T.E. Choe**, None; **W.O. Cepurna**, None; **J.C. Morrison**, None; **E.C. Johnson**, None

References

1. Sommer A. Intraocular pressure and glaucoma. *Am J Ophthalmol*. 1989;107:186–188.
2. Sommer A, Tielsch JM, Katz J, et al. Relationship between intraocular pressure and primary open angle glaucoma among white and black Americans. The Baltimore Eye Survey. *Arch Ophthalmol*. 1991;109:1090–1095.
3. Quigley HA, Addicks EM, Green WR, Maumenee AE. Optic nerve damage in human glaucoma. II. The site of injury and susceptibility to damage. *Arch Ophthalmol*. 1981;99:635–649.
4. Burgoyne CF. A biomechanical paradigm for axonal insult within the optic nerve head in aging and glaucoma. *Exp Eye Res*. 2011;93:120–132.
5. Kwon YH, Fingert JH, Kuehn MH, Alward WL. Primary open-angle glaucoma. *N Engl J Med*. 2009;360:1113–1124.
6. John SW, Smith RS, Savinova OV, et al. Essential iris atrophy, pigment dispersion, and glaucoma in DBA/2J mice. *Invest Ophthalmol Vis Sci*. 1998;39:951–962.
7. McLellan GJ, Teixeira LB. Feline glaucoma. *Vet Clin North Am Small Anim Pract*. 2015;45:1307–1333.
8. Rasmussen CA, Kaufman PL. Primate glaucoma models. *J Glaucoma*. 2005;14:311–314.
9. Burgoyne CF. The non-human primate experimental glaucoma model. *Exp Eye Res*. 2015.
10. Yuan L, Neufeld AH. Activated microglia in the human glaucomatous optic nerve head. *J Neurosci Res*. 2001;64:523–532.
11. Lam TT, Kwong JM, Tso MO. Early glial responses after acute elevated intraocular pressure in rats. *Invest Ophthalmol Vis Sci*. 2003;44:638–645.
12. Bosco A, Romero CO, Breen KT, et al. Neurodegeneration severity can be predicted from early microglia alterations monitored in vivo in a mouse model of chronic glaucoma. *Dis Model Mech*. 2015;8:443–455.
13. Tehrani S, Johnson EC, Cepurna WO, Morrison JC. Astrocyte processes label for filamentous actin and reorient early within the optic nerve head in a rat glaucoma model. *Invest Ophthalmol Vis Sci*. 2014;55:6945–6952.
14. Tehrani S, Davis L, Cepurna WO, et al. Astrocyte structural and molecular response to elevated intraocular pressure occurs rapidly and precedes axonal tubulin rearrangement within the optic nerve head in a rat model. *PLoS One*. 2016;11:e0167364.
15. Sun D, Lye-Barthel M, Masland RH, Jakobs TC. The morphology and spatial arrangement of astrocytes in the optic nerve head of the mouse. *J Comp Neurol*. 2009;516:1–19.
16. Wang R, Seifert P, Jakobs TC. Astrocytes in the optic nerve head of glaucomatous mice display a characteristic reactive phenotype. *Invest Ophthalmol Vis Sci*. 2017;58:924–932.
17. Sun D, Moore S, Jakobs TC. Optic nerve astrocyte reactivity protects function in experimental glaucoma and other nerve injuries. *J Exp Med*. 2017;214:1411–1430.
18. Johnson EC, Doser TA, Cepurna WO, et al. Cell proliferation and interleukin-6-type cytokine signaling are implicated by gene expression responses in early optic nerve head injury in rat glaucoma. *Invest Ophthalmol Vis Sci*. 2011;52:504–518.
19. Johnson EC, Jia L, Cepurna WO, Doser TA, Morrison JC. Global changes in optic nerve head gene expression after exposure to elevated intraocular pressure in a rat glaucoma model. *Invest Ophthalmol Vis Sci*. 2007;48:3161–3177.
20. Pazos M, Yang H, Gardiner SK, et al. Expansions of the neurovascular scleral canal and contained optic nerve occur early in the hypertonic saline rat experimental glaucoma model. *Exp Eye Res*. 2016;145:173–186.
21. Wu J, Li L, Jiang G, Zhan H, Wang N. B-cell CLL/lymphoma 3 promotes glioma cell proliferation and inhibits apoptosis through the oncogenic STAT3 pathway. *Int J Oncol*. 2016;49:2471–2479.
22. Kim DW, Glendining KA, Grattan DR, Jasoni CL. Maternal obesity leads to increased proliferation and numbers of astrocytes in the developing fetal and neonatal mouse hypothalamus. *Int J Dev Neurosci*. 2016;53:18–25.
23. Nakanishi M, Niidome T, Matsuda S, et al. Microglia-derived interleukin-6 and leukaemia inhibitory factor promote astrocytic differentiation of neural stem/progenitor cells. *Eur J Neurosci*. 2007;25:649–658.
24. Mi H, Haeberle H, Barres BA. Induction of astrocyte differentiation by endothelial cells. *J Neurosci*. 2001;21:1538–1547.
25. Bauer S. Cytokine control of adult neural stem cells. *Ann N Y Acad Sci*. 2009;1153:48–56.
26. Morrison JC, Moore CG, Deppmeier LM, et al. A rat model of chronic pressure-induced optic nerve damage. *Exp Eye Res*. 1997;64:85–96.
27. Morrison JC, Jia L, Cepurna W, Guo Y, Johnson E. Reliability and sensitivity of the TonoLab rebound tonometer in awake Brown Norway rats. *Invest Ophthalmol Vis Sci*. 2009;50:2802–2808.
28. Manikandan S. Data transformation. *J Pharmacol Pharmacother*. 2010;1:126–127.
29. Schlenker E. Tips and tricks for successful application of statistical methods to biological data. *Methods Mol Biol*. 2016;1366:271–285.
30. McDonald J. *Handbook of Biological Statistics*. Baltimore, MD: Sparky House Publishing; 2014.
31. Mangiafico SS. Summary and analysis of extension program evaluation in R, version 1.17.0. Available at: http://rcompanion.org/documents/RHandbookProgramEvaluation.pdf. Accessed February 20, 2019.
32. Johnson EC, Deppmeier LM, Wentzien SK, Hsu I, Morrison JC. Chronology of optic nerve head and retinal responses to elevated intraocular pressure. *Invest Ophthalmol Vis Sci*. 2000;41:431–442.
33. Shi Y, Sun G, Zhao C, Stewart R. Neural stem cell self-renewal. *Crit Rev Oncol Hematol*. 2008;65:43–53.
34. Kelley KW, Nakao-Inoue H, Molofsky AV, Oldham MC. Variation among intact tissue samples reveals the core transcriptional features of human CNS cell classes. *Nat Neurosci*. 2018;21:1171–1184.
35. Tiwari S, Dharmarajan S, Shivanna M, Otteson DC, Belecky-Adams TL. Histone deacetylase expression patterns in developing murine optic nerve. *BMC Dev Biol*. 2014;14:30.
36. Bennett ML, Bennett FC, Liddelow SA, et al. New tools for studying microglia in the mouse and human CNS. *Proc Natl Acad Sci U S A*. 2016;113:E1738–E1746.
37. Imai Y, Ibata I, Ito D, Ohsawa K, Kohsaka S. A novel gene iba1 in the major histocompatibility complex class III region encoding an EF hand protein expressed in a monocytic lineage. *Biochem Biophys Res Commun*. 1996;224:855–862.

Investigative Ophthalmology & Visual Science

38. Ito D, Imai Y, Ohsawa K, et al. Microglia-specific localisation of a novel calcium binding protein, Iba1. *Brain Res Mol Brain Res*. 1998;57:1–9.
39. Johnson EC, Cepurna WO, Choi D, Choe TE, Morrison JC. Radiation pretreatment does not protect the rat optic nerve from elevated intraocular pressure-induced injury. *Invest Ophthalmol Vis Sci*. 2014;56:412–419.
40. Lu QR, Yuk D, Alberta JA, et al. Sonic hedgehog–regulated oligodendrocyte lineage genes encoding bHLH proteins in the mammalian central nervous system. *Neuron*. 2000;25:317–329.
41. Young KM, Psachoulia K, Tripathi RB, et al. Oligodendrocyte dynamics in the healthy adult CNS: evidence for myelin remodeling. *Neuron*. 2013;77:873–885.
42. Zhou Q, Anderson DJ. The bHLH transcription factors OLIG2 and OLIG1 couple neuronal and glial subtype specification. *Cell*. 2002;109:61–73.
43. Zhou Q, Wang S, Anderson DJ. Identification of a novel family of oligodendrocyte lineage-specific basic helix-loop-helix transcription factors. *Neuron*. 2000;25:331–343.
44. Nicolas CS, Amici M, Bortolotto ZA, et al. The role of JAK-STAT signaling within the CNS. *JAKSTAT*. 2013;2:e22925.
45. Kim SY, Park HJ, Choi JS, et al. Ischemic preconditioning-induced expression of gp130 and STAT3 in astrocytes of the rat hippocampus. *Brain Res Mol Brain Res*. 2004;129:96–103.
46. Ceyzeriat K, Abjean L, Carrillo-de Sauvage MA, Ben Haim L, Escartin C. The complex states of astrocyte reactivity: How are they controlled by the JAK-STAT3 pathway? *Neuroscience*. 2016;330:205–218.
47. Morrison JC, Johnson EC, Cepurna W, Jia L. Understanding mechanisms of pressure-induced optic nerve damage. *Prog Retin Eye Res*. 2005;24:217–240.
48. Bullwinkel J, Baron-Luhr B, Ludemann A, et al. Ki-67 protein is associated with ribosomal RNA transcription in quiescent and proliferating cells. *J Cell Physiol*. 2006;206:624–635.
49. Schluter C, Duchrow M, Wohlenberg C, et al. The cell proliferation-associated antigen of antibody Ki-67: a very large, ubiquitous nuclear protein with numerous repeated elements, representing a new kind of cell cycle-maintaining proteins. *J Cell Biol*. 1993;123:513–522.
50. Gerdes J, Schwab U, Lemke H, Stein H. Production of a mouse monoclonal antibody reactive with a human nuclear antigen associated with cell proliferation. *Int J Cancer*. 1983;31:13–20.
51. Gerdes J, Lemke H, Baisch H, et al. Cell cycle analysis of a cell proliferation-associated human nuclear antigen defined by the monoclonal antibody Ki-67. *J Immunol*. 1984;133:1710–1715.
52. Knapp PE. The cell cycle of glial cells grown in vitro: an immunocytochemical method of analysis. *J Histochem Cytochem*. 1992;40:1405–1411.
53. Sobecki M, Mrouj K, Colinge J, et al. Cell-cycle regulation accounts for variability in Ki-67 expression levels. *Cancer Res*. 2017;77:2722–2734.
54. Butt AM, Pugh M, Hubbard P, James G. Functions of optic nerve glia: axoglial signalling in physiology and pathology. *Eye (Lond)*. 2004;18:1110–1121.
55. Son JL, Soto I, Oglesby E, et al. Glaucomatous optic nerve injury involves early astrocyte reactivity and late oligodendrocyte loss. *Glia*. 2010;58:780–789.
56. Qiu J, Zhang C, Lv Y, et al. Cdh1 inhibits reactive astrocyte proliferation after oxygen-glucose deprivation and reperfusion. *Neurochem Int*. 2013;63:87–92.
57. Huang XJ, Zhang WP, Li CT, et al. Activation of CysLT receptors induces astrocyte proliferation and death after oxygen-glucose deprivation. *Glia*. 2008;56:27–37.
58. Zhi Z, Cepurna WO, Johnson EC, Morrison JC, Wang RK. Impact of intraocular pressure on changes of blood flow in the retina, choroid, and optic nerve head in rats investigated by optical microangiography. *Biomed Opt Express*. 2012;3:2220–2233.
59. Zhi Z, Cepurna W, Johnson E, et al. Evaluation of the effect of elevated intraocular pressure and reduced ocular perfusion pressure on retinal capillary bed filling and total retinal blood flow in rats by OMAG/OCT. *Microvasc Res*. 2015;101:86–95.
60. Dihne M, Block F, Korr H, Topper R. Time course of glial proliferation and glial apoptosis following excitotoxic CNS injury. *Brain Res*. 2001;902:178–189.
61. Li T, Zhang S. Microgliosis in the injured brain: infiltrating cells and reactive microglia both play a role. *Neuroscientist*. 2016;22:165–170.
62. Wohl SG, Schmeer CW, Witte OW, Isenmann S. Proliferative response of microglia and macrophages in the adult mouse eye after optic nerve lesion. *Invest Ophthalmol Vis Sci*. 2010;51:2686–2696.
63. Fisher SK, Erickson PA, Lewis GP, Anderson DH. Intraretinal proliferation induced by retinal detachment. *Invest Ophthalmol Vis Sci*. 1991;32:1739–1748.
64. Horstmann L, Kuehn S, Pedreiturria X, et al. Microglia response in retina and optic nerve in chronic experimental autoimmune encephalomyelitis. *J Neuroimmunol*. 2016;298:32–41.
65. Noristani R, Kuehn S, Stute G, et al. Retinal and optic nerve damage is associated with early glial responses in an experimental autoimmune glaucoma model. *J Mol Neurosci*. 2016;58:470–482.
66. Qu J, Jakobs TC. The time course of gene expression during reactive gliosis in the optic nerve. *PLoS One*. 2013;8:e67094.
67. Bordone MP, Gonzalez Fleitas MF, Pasquini LA, et al. Involvement of microglia in early axoglial alterations of the optic nerve induced by experimental glaucoma. *J Neurochem*. 2017;142:323–337.
68. Ebneter A, Casson RJ, Wood JP, Chidlow G. Microglial activation in the visual pathway in experimental glaucoma: spatiotemporal characterization and correlation with axonal injury. *Invest Ophthalmol Vis Sci*. 2010;51:6448–6460.
69. O'Shea TM, Burda JE, Sofroniew MV. Cell biology of spinal cord injury and repair. *J Clin Invest*. 2017;127:3259–3270.
70. Robel S, Berninger B, Gotz M. The stem cell potential of glia: lessons from reactive gliosis. *Nat Rev Neurosci*. 2011;12:88–104.
71. Burda JE, Bernstein AM, Sofroniew MV. Astrocyte roles in traumatic brain injury. *Exp Neurol*. 2016;275(pt 3):305–315.
72. Norton WT. Cell reactions following acute brain injury: a review. *Neurochem Res*. 1999;24:213–218.
73. Amat JA, Ishiguro H, Nakamura K, Norton WT. Phenotypic diversity and kinetics of proliferating microglia and astrocytes following cortical stab wounds. *Glia*. 1996;16:368–382.
74. Xu W, Mu X, Wang H, et al. Chloride co-transporter NKCC1 inhibitor bumetanide enhances neurogenesis and behavioral recovery in rats after experimental stroke. *Mol Neurobiol*. 2017;54:2406–2414.
75. Tatsumi K, Haga S, Matsuyoshi H, et al. Characterization of cells with proliferative activity after a brain injury. *Neurochem Int*. 2005;46:381–389.
76. Mu S, Liu B, Ouyang L, et al. Characteristic changes of astrocyte and microglia in rat striatum induced by 3-NP and MCAO. *Neurochem Res*. 2016;41:707–714.
77. Quigley HA, Hohman RM, Addicks EM, Massof RW, Green WR. Morphologic changes in the lamina cribrosa correlated

Investigative Ophthalmology & Visual Science

with neural loss in open-angle glaucoma. *Am J Ophthalmol*. 1983;95:673–691.

78. Boassa D, Solan JL, Papas A, et al. Trafficking and recycling of the connexin43 gap junction protein during mitosis. *Traffic*. 2010;11:1471–1486.
79. Volterra A, Meldolesi J. Astrocytes, from brain glue to communication elements: the revolution continues. *Nat Rev Neurosci*. 2005;6:626–640.
80. Liu B, Teschemacher AG, Kasparov S. Neuroprotective potential of astroglia. *J Neurosci Res*. 2017;95:2126–2139.
81. Nortley R, Attwell D. Control of brain energy supply by astrocytes. *Curr Opin Neurobiol*. 2017;47:80–85.
82. Iadecola C. The neurovascular unit coming of age: a journey through neurovascular coupling in health and disease. *Neuron*. 2017;96:17–42.
83. Johnson EC, Morrison JC. Friend or foe? Resolving the impact of glial responses in glaucoma. *J Glaucoma*. 2009;18:341–353.
84. Bylicky MA, Mueller GP, Day RM. Mechanisms of endogenous neuroprotective effects of astrocytes in brain injury. *Oxid Med Cell Longev*. 2018;2018:6501031.
85. Sobieski C, Jiang X, Crawford DC, Mennerick S. Loss of local astrocyte support disrupts action potential propagation and glutamate release synchrony from unmyelinated hippocampal axon terminals in vitro. *J Neurosci*. 2015;35:11105–11117.
86. Gerkau NJ, Rakers C, Petzold GC, Rose CR. Differential effects of energy deprivation on intracellular sodium homeostasis in neurons and astrocytes. *J Neurosci Res*. 2017;95:2275–2285.
87. Ritchie JM. The oxygen consumption of mammalian non-myelinated nerve fibres. *J Physiol*. 1966;186:120P.
88. Bristow EA, Griffiths PG, Andrews RM, Johnson MA, Turnbull DM. The distribution of mitochondrial activity in relation to optic nerve structure. *Arch Ophthalmol*. 2002;120:791–796.
89. Barron MJ, Griffiths P, Turnbull DM, Bates D, Nichols P. The distributions of mitochondria and sodium channels reflect the specific energy requirements and conduction properties of the human optic nerve head. *Br J Ophthalmol*. 2004;88:286–290.
90. Inman DM, Harun-Or-Rashid M. Metabolic vulnerability in the neurodegenerative disease glaucoma. *Front Neurosci*. 2017;11:146.
91. Morgan JE. Circulation and axonal transport in the optic nerve. *Eye*. 2004;18:1089–1095.
92. Tabernero A, Jimenez C, Velasco A, Giaume C, Medina JM. The enhancement of glucose uptake caused by the collapse of gap junction communication is due to an increase in astrocyte proliferation. *J Neurochem*. 2001;78:890–898.
93. Mulukutla BC, Khan S, Lange A, Hu WS. Glucose metabolism in mammalian cell culture: new insights for tweaking vintage pathways. *Trends Biotechnol*. 2010;28:476–484.
94. Tsuda M, Kohro Y, Yano T, et al. JAK-STAT3 pathway regulates spinal astrocyte proliferation and neuropathic pain maintenance in rats. *Brain*. 2011;134(pt 4):1127–1139.
95. LeComte MD, Shimada IS, Sherwin C, Spees JL. Notch1-STAT3-ETBR signaling axis controls reactive astrocyte proliferation after brain injury. *Proc Natl Acad Sci U S A*. 2015;112:8726–8731.
96. Hong S, Song MR. STAT3 but not STAT1 is required for astrocyte differentiation. *PLoS One*. 2014;9:e86851.
97. Wong M, Li Y, Li S, et al. Therapeutic retrobulbar inhibition of STAT3 protects ischemic retina ganglion cells. *Mol Neurobiol*. 2015;52:1364–1377.
98. Su Z, Yuan Y, Cao L, et al. Triptolide promotes spinal cord repair by inhibiting astrogliosis and inflammation. *Glia*. 2010;58:901–915.
99. Tao Z, Cheng M, Wang SC, et al. JAK2/STAT3 pathway mediating inflammatory responses in heatstroke-induced rats. *Int J Clin Exp Pathol*. 2015;8:6732–6739.
100. Wang YF, Zu JN, Li J, et al. Curcumin promotes the spinal cord repair via inhibition of glial scar formation and inflammation. *Neurosci Lett*. 2014;560:51–56.
101. Song Y, Zeng Z, Jin C, et al. Protective effect of ginkgolide B against acute spinal cord injury in rats and its correlation with the Jak/STAT signaling pathway. *Neurochem Res*. 2013;38:610–619.
102. Yu L, Chen C, Wang LF, et al. Neuroprotective effect of kaempferol glycosides against brain injury and neuroinflammation by inhibiting the activation of NF-kappaB and STAT3 in transient focal stroke. *PLoS One*. 2013;8:e55839.
103. Wanner IB, Anderson MA, Song B, et al. Glial scar borders are formed by newly proliferated, elongated astrocytes that interact to corral inflammatory and fibrotic cells via STAT3-dependent mechanisms after spinal cord injury. *J Neurosci*. 2013;33:12870–12886.
104. Okada S, Nakamura M, Katoh H, et al. Conditional ablation of Stat3 or Socs3 discloses a dual role for reactive astrocytes after spinal cord injury. *Nat Med*. 2006;12:829–834.
105. Herrmann JE, Imura T, Song B, et al. STAT3 is a critical regulator of astrogliosis and scar formation after spinal cord injury. *J Neurosci*. 2008;28:7231–7243.
106. Quigley HA, Addicks EM, Green WR. Optic nerve damage in human glaucoma. III. Quantitative correlation of nerve fiber loss and visual field defect in glaucoma, ischemic neuropathy, papilledema, and toxic neuropathy. *Arch Ophthalmol*. 1982;100:135–146.
107. Kerrigan-Baumrind LA, Quigley HA, Pease ME, Kerrigan DF, Mitchell RS. Number of ganglion cells in glaucoma eyes compared with threshold visual field tests in the same persons. *Invest Ophthalmol Vis Sci*. 2000;41:741–748.
108. Yang H, He L, Gardiner SK, et al. Age-related differences in longitudinal structural change by spectral-domain optical coherence tomography in early experimental glaucoma. *Invest Ophthalmol Vis Sci*. 2014;55:6409–6420.
109. Agarwal R, Gupta SK, Agarwal P, Saxena R, Agrawal SS. Current concepts in the pathophysiology of glaucoma. *Indian J Ophthalmol*. 2009;57:257–266.
110. Morrison JC, Cepurna WO, Tehrani S, et al. A period of controlled elevation of IOP (CEI) produces the specific gene expression responses and focal injury pattern of experimental rat glaucoma. *Invest Ophthalmol Vis Sci*. 2016;57:6700–6711.
111. Surzenko N, Crowl T, Bachleda A, Langer L, Pevny L. SOX2 maintains the quiescent progenitor cell state of postnatal retinal Muller glia. *Development*. 2013;140:1445–1456.

Investigative Ophthalmology & Visual Science